

# Wave Propagation Analysis using High-Order Finite Element Methods: Spurious Oscillations excited by Internal Element Eigenfrequencies

D. Schmicker, S. Duczek, S. Liefold, U. Gabbert

*From a computational point of view, the numerical analysis of ultrasonic guided waves is still a very demanding task. Because of the high-frequency regime both a fine spatial and temporal discretization is required. To minimize the numerical costs, efficient and robust algorithms ought to be developed. One promising idea is therefore to focus on high-order finite element methods (ho-FEM).*

*The current article investigates the behavior of the  $p$ -version of the finite element method ( $p$ -FEM) and the spectral element method (SEM) with respect to the existence of spurious oscillations in the solution. Convergence studies have shown that it is possible to observe non-physical oscillations under certain conditions. These parasitic vibrations, however, significantly deteriorate the accuracy of the simulation. For this reason, we analyse this phenomenon in detail and propose solutions to avoid its occurrence.*

*Without loss of generality, we employ a two-dimensional plane strain model to derive a guideline as to how to avoid these spurious oscillations, placing a special emphasis on the relation between the element size, the polynomial degree of the high-order shape functions and the excitation frequency.*

*Our results show that accurate simulations are possible if the model is generated according to the proposed methodology. Moreover, the implementation of the guideline into an existing finite element software is straightforward; these properties turn the method into a useful tool for practical wave propagation analyses.*

## 1 Introduction

Wave propagation analysis can be divided into three main groups: (i) *seismic wave propagation*, (ii) *acoustic wave propagation*, and (iii) *guided wave propagation*. This article addresses the third topic, since it is closely related to structural health monitoring (SHM), which is of special interest to the authors. We expect, however, that the findings of the current article are applicable, without loss of generality, to the other classes of wave propagation problems.

The continuous monitoring of a structure aims to provide information on the structural integrity of the monitored region and to predict its residual life. The first step is to register the presence of a damage. The second step is to gather information on the possible location. The third step is accordingly to determine the extent and/or type of the damage before any details can be given about the residual life of the structure in the fourth and last step. SHM systems should, therefore, enable an online examination of safety-relevant structural components during operation. According to Worlton (1961) the application of ultrasonic waves for this purpose can be traced back to the early 60's. The development of suitable computational methods to predict and to evaluate the responses of ultrasonic waves interacting with defects is one of the major tasks in this area of research. Such models are of great importance, since they facilitate a better understanding of the interaction of guided waves with boundaries as well as with damages and support the design of reliable and robust signal processing methods. A finite element simulation of ultrasonic waves, however, calls for both a fine spatial discretization and temporal one (high frequency regime  $\rightarrow$  short wavelengths). As a consequence, a large number of degrees-of-freedom is required, resulting in disproportionate numerical costs. To this end, we have investigated alternative numerical approaches to solve the governing equations more efficiently. These methods comprise the mass-spring lattice model (MSLM) proposed by Baek and Yim (2011), the local interaction simulation approach (LISA) published by Lee and Staszewski (2007a,b), the spectral element method (SEM) presented by Patera (1984), Komatitsch and Tromp (2002), Ha and Chang (2010), and the  $p$ -version of the finite element method ( $p$ -FEM) proposed by Babuška et al. (1981) and further developed by Düster (2002), Willberg et al. (2012), and Duczek and Gabbert (2013). By way of reference, Willberg et al. (2012) introduced some discussions about high-order finite element methods seeming to be the most viable choice to deal with practice-oriented problems including ultrasonic guided waves. The following paragraphs will therefore take a closer look at the properties of *ho*-FEM in the context of wave propagation analysis.

During the past few decades, several authors analyzed the accuracy and the numerical/grid dispersion inherent to finite element approaches when solving the wave equation (both acoustic and elastic). Grid dispersion describes a phenomenon where numerical noise related to the grid spacing causes dispersion. This, of course, has a detrimental effect on the accuracy of the wave propagation analysis (De Basabe and Sen, 2007). The reason for the described numerical dispersion is the mismatch between the actual velocity of high-frequency waves in the grid and the true velocity. As the grid is the source of this error, the name numerical or grid dispersion was coined for this phenomenon. We also wish to point out that it also occurs when the physical problem being solved is not dispersive. It can only be controlled by choosing an appropriate element size and time-step (De Basabe and Sen, 2007).

The first systematic studies of the properties of finite element methods ( $p$ -FEM) for high wavenumber applications, however, were carried out in a series of papers by Ihlenburg and Babuška (1995a,b, 1997b,a). They present new error estimates for solving the wave equation and conclude that it is not possible to totally eliminate the phase error. It is, however, still possible to achieve significant error reductions by means of a suitable discretization depending on the wavenumber. The same authors also state that the choice of shape functions is irrelevant from the point of view of the dispersive characteristics of the numerical solution, again highlighting the importance of high-order shape functions. They found that high-order finite elements exhibit a greater degree of accuracy than low order finite elements for the same number of degrees-of-freedom. According to Ihlenburg and Babuška (1995a,b, 1997b,a), the most significant improvements in accuracy are obtained when transferring the standard  $h$ -version (with  $p = 1$ ) to approximation order  $p = 2$  or  $p = 3$ .

Seriani and Priolo (1994) made similar observations regarding the spectral element method. They found that the results are more accurate compared to those of low-order finite elements. Based on their research, Seriani and Priolo (1994) concluded that there is a theoretical limit to the number of nodes per minimum wavelength of  $\pi$  for an increasing polynomial degree. In this case, the accuracy remains almost unchanged even for long propagation times. For practical applications they recommend 4.5 nodes per wavelength deploying a polynomial degree of  $p = 8$ . As a practical rule of thumb, they state that using at least 4 nodes per wavelength for the spatial resolution and a polynomial degree of  $p = 4$  significantly reduces the numerical dispersion error. If longer wave propagation periods are to be investigated, higher polynomial orders are needed to avoid error accumulation and numerical anisotropy (Seriani, 1998; Seriani and Oliveira, 2008a). De Basabe and Sen (2007) compare the dispersion properties of FEM and SEM. Both formulations are used to discretize the acoustic and elastic wave equation. The analysis reveals that the dispersion error can be reduced below 0.2% for SEM of order four or greater with at least 5 nodes per wavelength.

Jensen (1996), Dauksher and Emery (1999, 1997), Christon (1999) and Ainsworth and Wajid (2010a,b) comment on the influence the mass matrix has on the numerical results. Jensen (1996) deploys the spectral element method with a diagonalized mass matrix. He concludes that mass lumping does not introduce additional errors. In the case of spectral elements based on a Gauss-Lobatto-Legendre (GLL) grid, a simple nodal quadrature (GLL-quadrature rule) provides an elegant way to diagonalize the mass-matrix. Komatitsch and Tromp (2002) offer similar conclusions and recommend a polynomial degree of  $p = 4/5$  since, from their point of view, it provides the best trade-off between accuracy and integration stability. By way of reference, Christon (1999) showed that the higher order mass matrix - a linear combination of lumped and consistent mass matrices - can improve the dispersion characteristics of both reduced and fully integrated finite elements. Ainsworth and Wajid (2010a,b) also utilized a weighted average of the consistent and diagonalized mass matrices. They demonstrate that the optimal blending parameter for finite elements of order  $p$  is given by the ratio  $1 : p$ . Compared to the pure schemes additional two orders of accuracy can be gained independent of the spatial dimensions. An efficient implementation of the higher order mass matrix can be achieved by nonstandard integration rules. An explicit construction of the nodes and weights is given in Ainsworth and Wajid (2010b). Ainsworth and Wajid (2010a) also find  $\pi$  as a theoretical limit for the number of nodes per wavelength if the polynomial degree is increased accordingly (previously stated by Seriani and Priolo (1994)). Dauksher and Emery (1999, 1997) demonstrated that a row-summing procedure can result in accurate solutions with spectral elements based on Chebyshev points (GLC). This row-summing procedure is only performed on the global mass matrix. Nonetheless, the solution characteristics are relatively unaffected by the diagonalized mass matrix but the numerical costs of solving of the equation system is drastically reduced when applying an explicit time-integration scheme. The authors opt for deploying row-summed mass matrix spectral elements with central time differencing to solve the wave equation.

The angle-dependency of the wave propagation properties has been studied by Mullen and Belytschko (1982), Christon (1999) and De Basabe and Sen (2007) for example. Mullen and Belytschko (1982) noticed the angle-dependency for linear two-dimensional finite elements and observed a higher dispersion error when the stiffness matrix is underintegrated. De Basabe and Sen conclude that SEM is clearly advantageous and that the dispersion results gathered for the acoustic case can be transferred to the elastic case.

Mulder (1999) investigates spurious or parasitic modes that can occur if high-order finite elements are used to discretize the wave equation (SEM:  $p = 2, \dots, 6$ ). The Fourier analysis is used to study the aforementioned phe-

nomenon. No deleterious effects are produced for a high enough polynomial degree. He recommends employing spectral elements based on a GLL grid with a diagonalized mass matrix. Park and Flaggs (1984) defined spurious mechanisms as non-physical oscillatory components that are intrinsic in the spatial discretization regardless of the uniformity of the mesh spacing. They are often associated with rank deficiencies of the element stiffness matrix. The goal of their investigations is to develop a technique to identify these phenomena as intrinsic element properties. These studies were carried out on a one-dimensional axial bar. Abboud and Pinsky (1992) investigated standard finite elements (8-node trilinear element, 20-node serendipity element, 27-node tri-quadratic element). The results of their analysis indicate that the serendipity element is not suitable for wave propagation analysis in terms of simplicity and accuracy. It is more complex and does not offer the same numerical economy as the 8-node element, nor does it exhibit the same accuracy as the 27-node tri-quadratic finite element. Seriani and Oliveira (2008b) study spectral elements based on a GLL and GLC grid. They observe the following properties: spectral elements using a GLC grid exhibit a phase lead, while GLL-based spectral elements produce lagging errors. Ainsworth and Wajid (2010b) and Thompson and Pinsky (1994) recorded similar findings for lumped and consistent mass matrix formulations. Thompson and Pinsky employ the Fourier analysis technique to examine the dispersion in  $p$ -version finite elements up to order  $p = 5$ . They use the term  $p$ -version of FEM differently than it is normally understood. They considered hierarchic Legendre basis functions ( $p$ -FEM), hierarchic Fourier basis functions (Fourier  $p$ -FEM Leung and Chan (1997); Leung and Zhu (2003)) and spectral basis functions based on Gauss-Lobatto-Legendre points (SEM). Thompson and Pinsky again confirm the well-known fact that clearly high-order  $p$ -type elements exhibit increased accuracy compared to low order finite elements, for the same number of degrees-of-freedom. To resolve the wavefront, they claim that two elements per wavelength are sufficient for polynomial degrees of  $p \geq 4$ . Conclusions from their study are that, for well-resolved waves, SEM produces better results in terms of phase error when compared to hierarchic elements. For higher frequencies, however, both dispersion and amplitude attenuation errors increase the most. Ainsworth (2004) proves that the error decay is quasi-optimal when the number of nodes per wavelength is greater than  $\pi$ .

Regarding the literature survey on dispersion errors and spurious modes, we note that no practical guidelines have been proposed to circumvent these deleterious effects. The given error estimates are necessary for adaptive solution techniques but are hard to use for an a priori determination of the appropriate discretization set-up. The articles dealing with spurious effects concentrate almost exclusively on one-dimensional structures. Provided we accept the definition of spurious waves given by Park and Flaggs (1984), we will show in the course of the investigations throughout the current paper that the described effect is very different in nature from what has previously been reported in literature.

The effect we describe in this paper is of practical importance when examining typical thin-walled structures (aeronautics, aerospace). We therefore propose to use an engineering approach instead of a mathematically thorough treatment of the observed effect. The present paper deals with a phenomenon that was discovered in Willberg et al. (2012), who observed that stationary, non-physical oscillations occur in specific cases. The following sections investigate the reasons for this effect in detail. The said phenomenon can be of crucial importance, particularly when thinking about designing signal-processing algorithms for SHM-systems on the basis of numerical high-order models. Consequently, following comprehensive investigations, we propose a guideline to determine an appropriate discretization to avoid this special kind of spurious oscillations.

The outline of the paper is as follows: Section 2 briefly recalls the basic principles of the finite element method and introduces two types of high-order shape functions related to the  $p$ -version of FEM and SEM. A short introduction to ultrasonic guided waves, especially Lamb waves, is given in Section 3. This is followed by a description of the numerical model in Section 4, which serves to illustrate the observed phenomenon. To determine the cause of these spurious oscillations, an eigenvalue analysis is conducted in Section 5, after which we elaborate a guideline to avoid this phenomenon. Finally, Section 6 summarizes the main points and provides conclusions.

## 2 High-Order Finite Element Methods

The following section briefly recalls the fundamentals of the finite element methods. All fundamental principles are identical. The only difference is to be seen in the shape functions employed. In the current article, however, we confine our analysis to wave propagation problems in linear elastic, isotropic and homogeneous materials. All quantities are given in Voigt-notation. Therefore, the here applied matrix notation understands vectors as component representations of physical quantities or numerical parameters being arranged to column format. Hence, products of vectors and/or matrices are abbreviations of component sums according to Falk's scheme. The product  $\mathbf{a}^T \mathbf{b}$ , for instance, refers to the scalar product  $\sum_i a_i b_i$ .

## 2.1 Basic Principles

The finite element developments are based on the variational formulation corresponding to Navier's equations, namely Hamilton's principle. It states that the motion of the system within the time interval  $[t_1, t_2]$  is such that, under infinitesimal variations of the displacements, the Hamiltonian action  $S_H$  vanishes, meaning that the motion of the system follows the path of the stationary action (Hamel, 1967)

$$\delta S_H = \delta \int_{t_1}^{t_2} (L + W_E) dt = 0. \quad (1)$$

Here  $L$  represents the Lagrangian function, and  $W_E$  the work done by the external forces. The Lagrangian is the difference between the kinetic energy  $K$  and the elastic strain energy  $W_I$  ( $L = K - W_I$ ). After some calculations and the substitution of Hooke's law into Eq. (1), the variational formulation takes the following form

$$0 = - \underbrace{\int_{\Omega} [\rho \delta \mathbf{u}^T \ddot{\mathbf{u}} + \delta \boldsymbol{\varepsilon}^T \mathbf{C} \boldsymbol{\varepsilon}] d\Omega}_{\delta L} + \underbrace{\int_{\Omega} \delta \mathbf{u}^T \mathbf{F}_V d\Omega + \int_{\Gamma} \delta \mathbf{u}^T \mathbf{F}_S d\Gamma}_{\delta W_E}, \quad (2)$$

where  $\rho$  is the mass density,  $\boldsymbol{\varepsilon}$  and  $\boldsymbol{\sigma}$  are the vectors of mechanical strains and stresses in Voigt notation, respectively (Zienkiewicz and Taylor, 2000a).  $\mathbf{C}$  denotes the elasticity matrix and  $\ddot{\mathbf{u}}$  represents the acceleration vector. The external forces can be divided into surface loads  $\mathbf{F}_S$  and volume loads  $\mathbf{F}_V$ .  $\Omega$  and  $\Gamma$  represent the computational domain and its boundary, respectively. If we divide the domain of interest into several elements, then the displacement field  $\mathbf{u}(\mathbf{x}, t)$  in each finite element, denoted by  $e$ , is approximated by the product of the space-dependent shape function matrix  $\mathbf{N}_e(\mathbf{x})$  and a time-dependent vector of unknowns  $\mathbf{U}_e(t)$ ,

$$\mathbf{u}(\mathbf{x}, t) = \mathbf{N}_e(\mathbf{x}) \mathbf{U}_e(t). \quad (3)$$

The mechanical strain is defined as

$$\boldsymbol{\varepsilon} = \mathcal{D} \mathbf{N}_e \mathbf{U}_e = \boldsymbol{\mathcal{B}}_e \mathbf{U}_e, \quad (4)$$

by introducing the strain-displacement matrix as  $\boldsymbol{\mathcal{B}}_e = \mathcal{D} \mathbf{N}_e$ , where  $\mathcal{D}$  is a linear differential operator relating strains and displacements. With the aid of Eqs. (2), (3) and (4) and the reasoning that Hamilton's principle has to be satisfied for all variations  $\delta \mathbf{u}_e = \mathbf{N}_e \delta \mathbf{U}_e$ , we obtain the well-known equation of motion

$$\mathbf{M}_g \ddot{\mathbf{U}}_g + \mathbf{K}_g \mathbf{U}_g = \mathbf{f}_g \quad (5)$$

where the system matrices are obtained by assembling all element matrices

$$\mathbf{M}_g = \mathbf{A} \sum_{e=1}^{n_e} \mathbf{M}_e, \quad (6)$$

$$\mathbf{K}_g = \mathbf{A} \sum_{e=1}^{n_e} \mathbf{K}_e, \quad (7)$$

$$\mathbf{f}_g = \mathbf{A} \sum_{e=1}^{n_e} \mathbf{f}_e. \quad (8)$$

The elemental mass and stiffness matrix as well as the elemental load vector are given as

$$\mathbf{M}_e = \int_{\Omega_e} \rho \mathbf{N}_e^T \mathbf{N}_e d\Omega, \quad (9)$$

$$\mathbf{K}_e = \int_{\Omega_e} \boldsymbol{\mathcal{B}}_e^T \mathbf{C} \boldsymbol{\mathcal{B}}_e d\Omega, \quad (10)$$

$$\mathbf{f}_e = \int_{\Omega_e} \mathbf{N}_e^T \mathbf{F}_{eV} d\Omega + \int_{\Gamma_e} \mathbf{N}_e^T \mathbf{F}_{eS} d\Gamma, \quad (11)$$

where  $\Omega_e$  and  $\Gamma_e$  are the domain of a single element and its corresponding boundary. For further explanations, such as including the influence of damping in the finite element method, the reader should refer to standard text-books on this subject by Zienkiewicz and Taylor (2000a,b,c), Wriggers (2009), Bathe (2002), Fish and Belytschko (2007) and Hughes (1987), for instance.

## 2.2 Shape Functions

This section discusses two different types of  $p$ -extensions. We begin by introducing the hierarchic Legendre basis functions (Weinberg, 1996; Düster, 2002; Solin et al., 2004; Demkowicz, 2006; Demkowicz et al., 2008), before presenting the Lagrange interpolation polynomials defined on a Gauss-Lobatto-Legendre grid (GLL) (Komatitsch and Tromp, 2002; Ha and Chang, 2010; Zak et al., 2006; Kudela et al., 2006; Peng et al., 2009). The first approach is commonly referred to as the  $p$ -version of the finite element method ( $p$ -FEM) while the latter one is known as spectral element method (SEM). Both methods are very accurate and suitable for wave propagation analysis. It has been thoroughly demonstrated that under certain conditions these approaches exhibit an exponential convergence rate in the energy norm (Düster, 2002; Pozrikidis, 2005; Fichtner, 2011).

### 2.2.1 Hierarchic Legendre Polynomials

The definition of the shape functions, based on the normalized integral of the Legendre polynomials, follows the procedure described in the monograph by Szabó and Babuška (1991, 2011). We start with the standard linear shape functions, also referred to as nodal shape functions

$$N_i^{\text{Legendre}}(\xi) = \frac{1}{2}(1 + \xi_i \xi), \quad i = 1, 2, \quad (12)$$

where  $\xi_i$  is the local coordinate of the  $i^{\text{th}}$  node. High-order shape functions are added to the set in a hierarchical fashion. They are defined in terms of the normalized integrals of the Legendre polynomials

$$N_i^{\text{Legendre}}(\xi) = \frac{1}{\|L_{i-2}\|} \int_{x=-1}^{\xi} L_{i-2}(x) dx, \quad i = 3, 4, \dots, p+1, \quad (13)$$

with the norm of the Legendre polynomial

$$\|L_{i-2}\| = \sqrt{\frac{2}{2i-3}}. \quad (14)$$

These functions have the property that  $N_i^{\text{Legendre}}(\mp 1) = 0$ . The corner nodes ( $i = 1, 2$ ) consequently retain a physical meaning, whereas the internal variables ( $i = 3, 4, \dots, p+1$ ) cannot be interpreted physically. The degrees-of-freedom are therefore connected to modes. Moreover, we have to keep in mind that this set of shape functions is hierarchic, cf. Fig. 1. The resulting element matrices and vectors are accordingly likewise hierarchic in the sense that the matrix corresponding to polynomial degree  $p$  is a sub-set of the matrix corresponding to order  $p+1$ . This property is of great help in adaptive  $p$ -refinement procedures. The first four shape functions are depicted shown in Fig. 1 by way of an example.

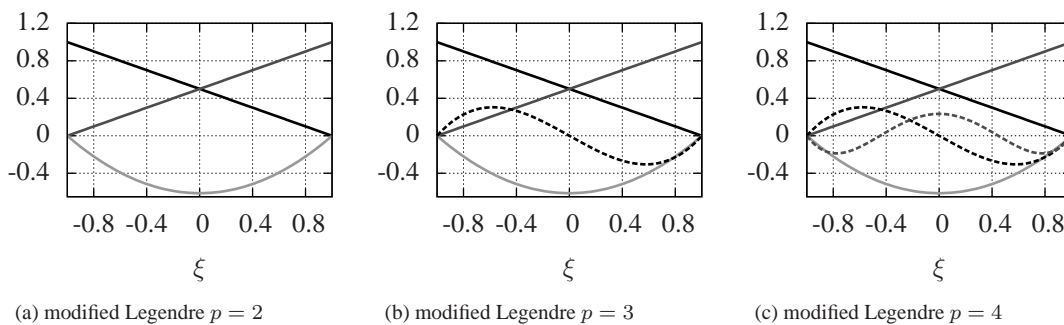


Figure 1: One-dimensional shape functions for the  $p$ -version of the finite element method. Normalized integrals of the Legendre polynomials.

### 2.2.2 Lagrange Polynomials

The presentation of the spectral shape functions is based on the implementation discussed in the monograph by Ostachowicz et al. (2011). These  $p$ -type elements (Thompson and Pinsky, 1994) are based on Lagrange interpolation polynomials defined on a GLL nodal distribution. The Gauss-Lobatto points ( $\xi_j, j = 1, \dots, (p + 1)$ ) are defined in such a way that

$$\xi_j = \begin{cases} -1 & \text{if } j = 1 \\ \xi_{0,j-1}^{Lo,p-1} & \text{if } 2 \leq j \leq p \\ +1 & \text{if } j = p + 1 \end{cases} . \quad (15)$$

Here  $\xi_{0,n}^{Lo,p-1}$  ( $n = 1, \dots, (p - 1)$ ) denotes the roots of the  $(p - 1)^{th}$ -order Lobatto polynomial

$$Lo_{p-1}(\xi) = \frac{1}{2^p p!} \frac{d^{p+1}}{d\xi^{p+1}} [(\xi^2 - 1)^p] . \quad (16)$$

Therefore, the basis functions based on Lagrange polynomials are given by

$$N_i^{Lagrange,p}(\xi) = \prod_{j=1, j \neq i}^{p+1} \frac{\xi - \xi_j}{\xi_i - \xi_j}, \quad i = 1, 2, \dots, p + 1. \quad (17)$$

In this case, all degrees-of-freedom retain their physical meaning. The degrees-of-freedom are therefore connected to nodes. If a GLL grid is used in conjunction with the Gauss-Lobatto quadrature, the elemental mass matrix is under-integrated and diagonalized. This is due to the fact that the integration points coincide with the nodal coordinates. We wish to point out, however, that this set of shape functions is not hierarchical by construction. The first four shape functions are shown in Fig. 2 by way of an example.

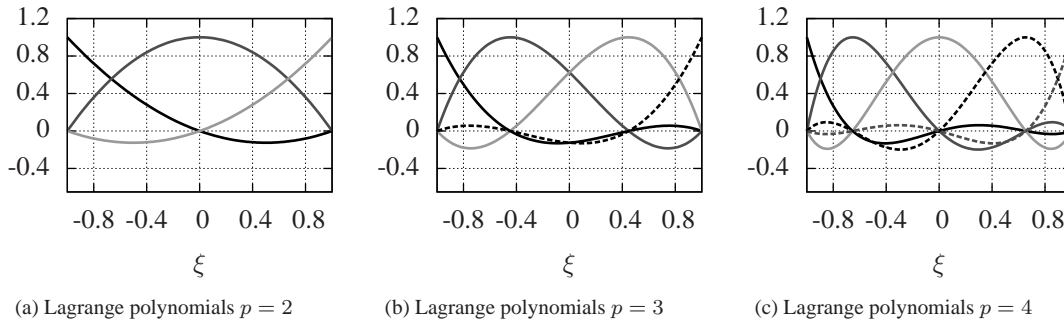
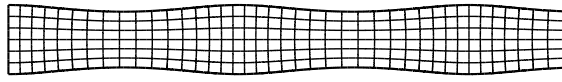


Figure 2: One-dimensional shape functions for the spectral element method. Lagrange interpolation polynomials through Gauß-Lobatto-Legendre points.

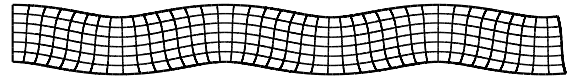
For a detailed discussion of the spectral methods the interested reader is referred to the monographs by Ostachowicz et al. (2011), Fichtner (2011) and Pozrikidis (2005).

### 3 Ultrasonic guided Wave

The propagation of elastic waves in solid media is the subject of many textbooks: Viktorov (1967); Graff (1975); Achenbach (1987); Rose (1999); Giurgiutiu (2008); Su and Ye (2009); Eds.: Boller et al. (2009); Raghavan and Cesnik (2005). This treatise is of particular interest in guided elastic waves. Lamb waves are one important representative of this class of waves. They propagate in plate- and shell-like structures with free surfaces and are a type of ultrasonic, dispersive waves. The term was coined in honor of its discover Horace Lamb, who was the first to describe them mathematically in his seminal work “On Waves in an Elastic Plate” Lamb (1917). The first comprehensive book on this subject was published by Viktorov (1967) and is now regarded as the standard text on Lamb wave propagation.



(a)  $S_0$ -mode with a phase velocity of  $c_p = 5.248$  km/s



(b)  $A_0$ -mode with a phase velocity of  $c_p = 2.464$  km/s

Figure 3: The two fundamental Lamb wave modes encountered in an aluminum plate (material data: Tab. 1) at  $fd = 1.25$  MHz mm.

Through multiple reflections on the plate's lower and upper surfaces, and through constructive and destructive interference, pressure waves (primary/P-waves) and shear waves (secondary/S-waves) give rise to Lamb waves, which consist of a pattern of standing waves in the  $z$ -(thickness)-direction (Lamb wave modes) behaving like travelling waves in the  $x$ -direction Giurgiutiu (2008). Accordingly, two different types of Lamb waves can be distinguished; symmetric  $S_i$ - and anti-symmetric  $A_i$ -modes, cf. Fig. 3. The terms symmetric and anti-symmetric refer to the  $u_z$  displacement component, cf. Figs. 3. The out-of-plane displacement is symmetric with respect to the mid-plane for symmetric modes and anti-symmetric for anti-symmetric modes. Besides being multi-modal, Lamb waves also display a dispersive behaviour, i.e. their properties - such as the group velocity - are frequency-dependent, cf. Fig. 4. To be exact, the velocity does not only depend on the frequency but on the product of the excitation frequency and the thickness ( $f \cdot d$ ) of the structure. For a more detailed review of ultrasonic guided waves the reader is referred to the aforementioned literature.

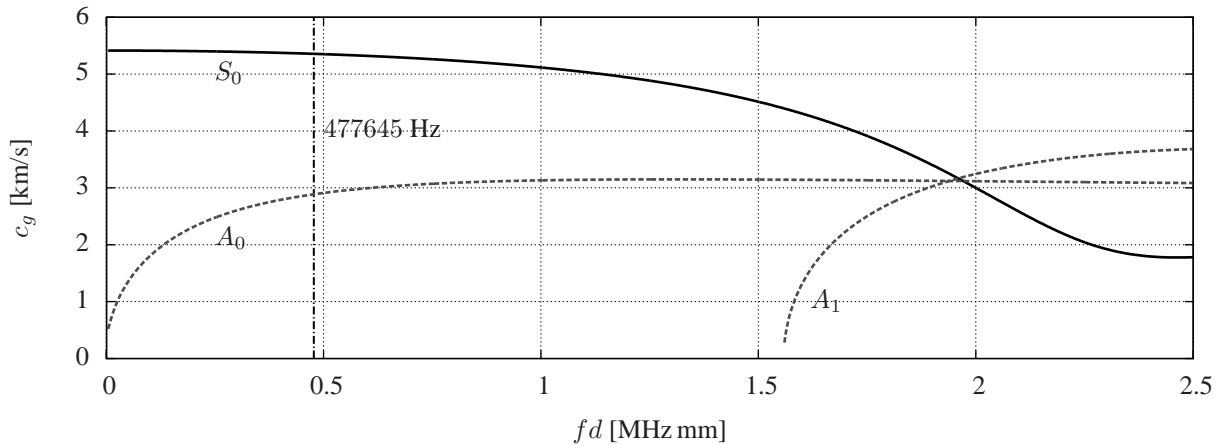


Figure 4: Group velocity dispersion diagram for a linear elastic, isotropic material ( $\lambda_L = 5.1084 \cdot 10^{10}$  N/m<sup>2</sup>,  $\mu = 2.6316 \cdot 10^{10}$  N/m<sup>2</sup> and  $\rho = 2700$  kg/m<sup>3</sup>; aluminum). Dashed lines denote anti-symmetric Lamb wave modes, while solid lines represent symmetric modes.

#### 4 Benchmark Problem

During the investigation of the convergence properties of different high-order finite element methods, distinct peaks in the convergence curves have been observed, cf. Willberg et al. (2012). Therefore, the main objective of the current article is to investigate the reasons for their occurrence. In doing so, we are able to propose measures to avoid this phenomenon.

At this point, for the sake of completeness, we briefly describe the numerical model employed by Willberg et al. (2012). Without loss of generality, a two-dimensional plane strain model is used. The geometry and boundary conditions are depicted in Fig. 5.

Generally, a mono-modal excitation is favored. This technique allows us to study the properties and the behavior of symmetric and anti-symmetric Lamb waves separately. To this end, the excitation is conducted using a pair of collocated point forces. This, however, makes it easier to interpret the signal. These loads are applied at the top and bottom surface  $x = 0$ . Depending on the choice of parameter  $\nu = \pm 1$  either only symmetric or only

anti-symmetric wave packets are excited. The excitation signal is a windowed (Hann-window) sine burst signal

$$F(t) = \begin{cases} \hat{F} \sin(2\pi f_D t) \sin^2\left(\frac{\pi f_D t}{n_D}\right) & \text{if } 0 \leq t \leq \frac{n_D}{f_D}, \\ 0 & \text{if } t > \frac{n_D}{f_D}, \end{cases} \quad (18)$$

where  $n_D$  is the number of cycles,  $\hat{F}$  represents the signal amplitude and  $f_D$  denotes the center frequency.

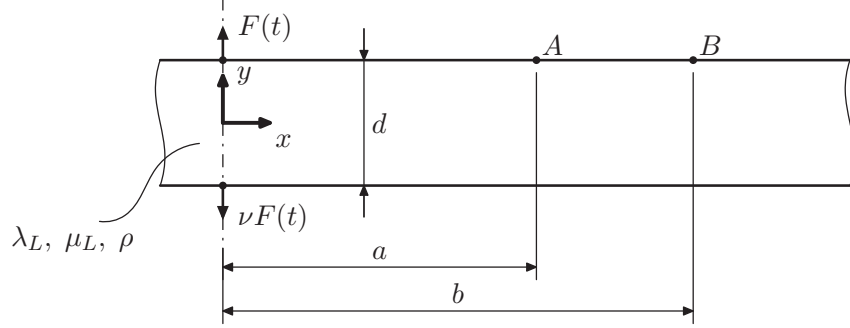


Figure 5: Analytical model for the convergence study.

Due to the symmetry of the model, we only discretize one half of the plate using high-order finite elements and apply symmetry boundary conditions, cf. Fig. 6. The plate length is chosen in such a way that reflections at the right boundary do not interfere with the signals measured at the evaluation points A and B. The spatial discretization is characterized by the polynomial degree of the shape functions in propagation direction  $p_x$ , the polynomial order in thickness direction  $p_y$  and the element width  $b_e$ .

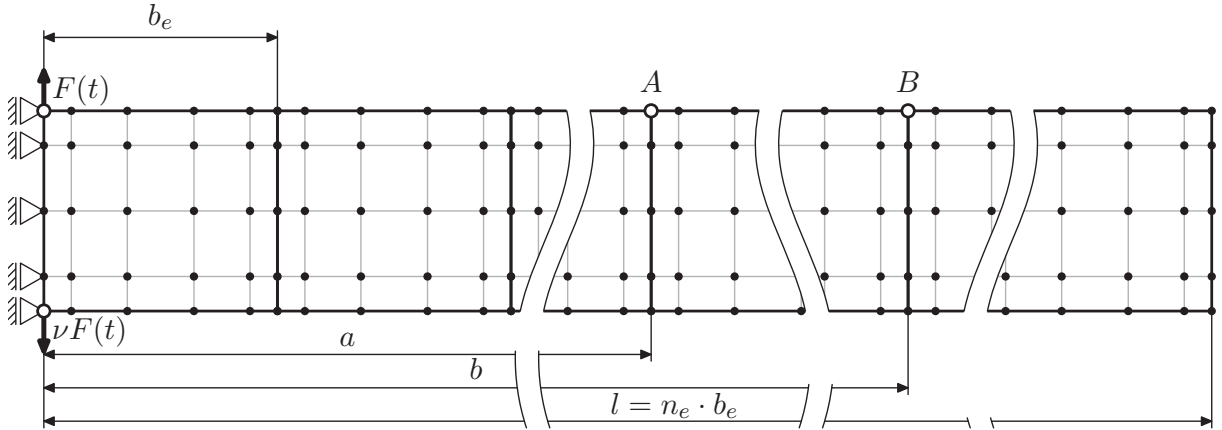


Figure 6: Numerical model for the convergence study.

The time-of-flight  $t_c$  between points A and B is evaluated. Since the distance between these points is known a priori,  $t_c$  corresponds to the group velocity  $c_g$  of the simulated wave packet. The analytical values  $c_{g,exact}$  can be taken from Achenbach (1987).

To determine the time-of-flight for the numerical models, we employ the Hilbert-transform. First, we calculate the envelopes of the time signals at points A and B. Secondly, we compute the centroids of those curves, cf. Fig. 7. Proceeding in this way, we determine the times-of-flight from the origin to the evaluation points. The relevant values suggest the  $t_{c,num}$  (Willberg et al., 2012; Xu et al., 2009). The relative error can, therefore, be determined by

$$E_{rel} = \frac{|c_{g,num} - c_{g,exact}|}{c_{g,exact}}. \quad (19)$$

Each simulation uses a distinct polynomial degree template  $p_x$  and  $p_y$ , while the element width  $b_e$  is successively decreased ( $h$ -refinement). In order to gain a dimensionless refinement parameter to evaluate the results, we introduce the number of modes/nodes per wavelength ( $\chi_{S_0}$ )

$$\chi_{S_0} = \frac{p_x}{b_e} \lambda. \quad (20)$$

Here,  $\lambda$  is the wavelength,  $c_g$  stands for the group velocity and is a function of  $f \cdot d$ ,  $\lambda_L$  and  $\mu$  represent the two Lamé constants and the mass density is denoted by  $\rho$ . The model parameters are compiled in Table 1.

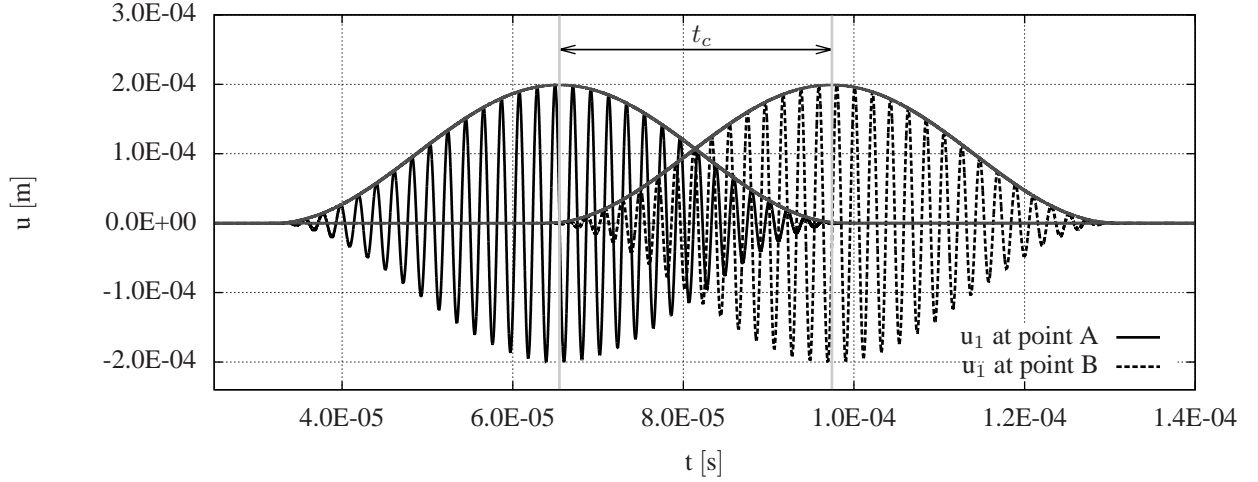


Figure 7: Computation of the time-of-flight between points A and B.

Table 1: Model parameter for the convergence study.

Parameter name	Symbol	Value
1st Lamé constant	$\lambda_L$	$5.1084 \cdot 10^{10}$ N/m <sup>2</sup>
2nd Lamé constant	$\mu_L$	$2.6316 \cdot 10^{10}$ N/m <sup>2</sup>
Center frequency	$f_D$	477465 Hz
Group speed	$c_{g,sym,exact}$	5147.9 m/s
Group speed	$c_{g,asym,exact}$	3130.0 m/s
Wavelength $S_0$ -Mode	$\lambda_{sym}$	0.0111362 m
Wavelength $A_0$ -Mode	$\lambda_{asym}$	0.00481439 m
Amplitude	$\hat{F}$	$1 \cdot 10^7$ N
Number of cycles	$n_D$	32
Mass density	$\rho$	2700 kg/m <sup>3</sup>
Plate thickness	$d$	0.002 m
Distance to point A	$a$	0.03 m
Distance to point B	$b$	0.1 m

Time integration is performed with a Runge-Kutta algorithm of fourth order including an adaptive time-step control. A time-integration scheme from the Runge-Kutta family is deployed in order to demonstrate that the said effect occurs independently of the numerical time-marching algorithm. Note that the numerical quadrature of stiffness and mass matrices is exact due to the fact that a regular mesh with undistorted rectangular elements is employed. Mass matrix diagonalization (lumping) methods are not applied in this investigation.

In the remainder of the current section only the results for the symmetric Lamb wave mode are discussed. Without loss of generality, the  $h$ -refinement is conducted for several polynomial degree templates  $p_x$  and  $p_y$ . The results of the convergence study for the SEM are depicted in Fig. 8. As we can see, the convergence behavior is significantly disrupted at points where the amount of nodes per wavelength  $\chi_{S_0}$  is a multiple of the shape function degree  $p_x$ . Similar observations are made by studying the anti-symmetric Lamb wave mode, other polynomial degrees in thickness direction, or different excitation frequencies  $f_D$ , respectively. These statements also hold if the  $p$ -version of FEM is employed to discretize the benchmark problem, cf. Fig. 9. Willberg (2013) shows that these peaks can also be observed for  $C_0$ -continuous isogeometric finite elements. So it is safe to say that this problem is inherent to all  $C_0$ -continuous finite elements regardless of the chosen polynomial degree.

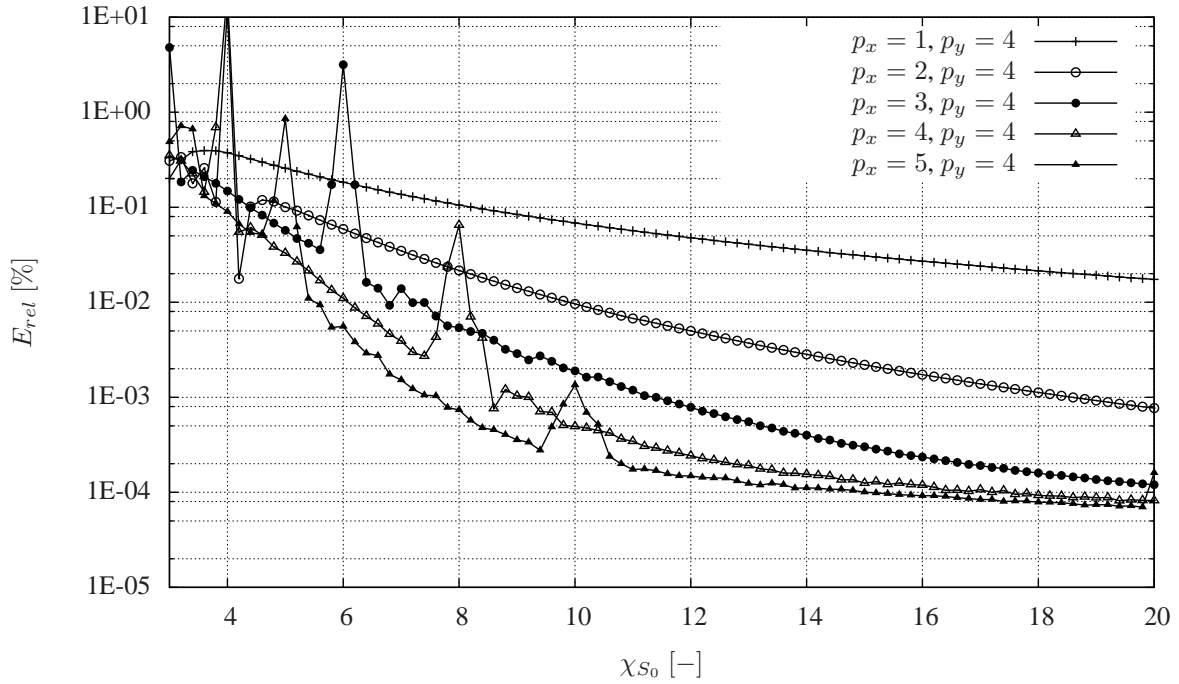


Figure 8: Results of the convergence study for the fundamental symmetric Lamb wave mode are depicted. The model has been discretized using spectral elements. The relative error in group velocity is given over the number of nodes per symmetric wavelength ( $\lambda_{S_0}$ ).

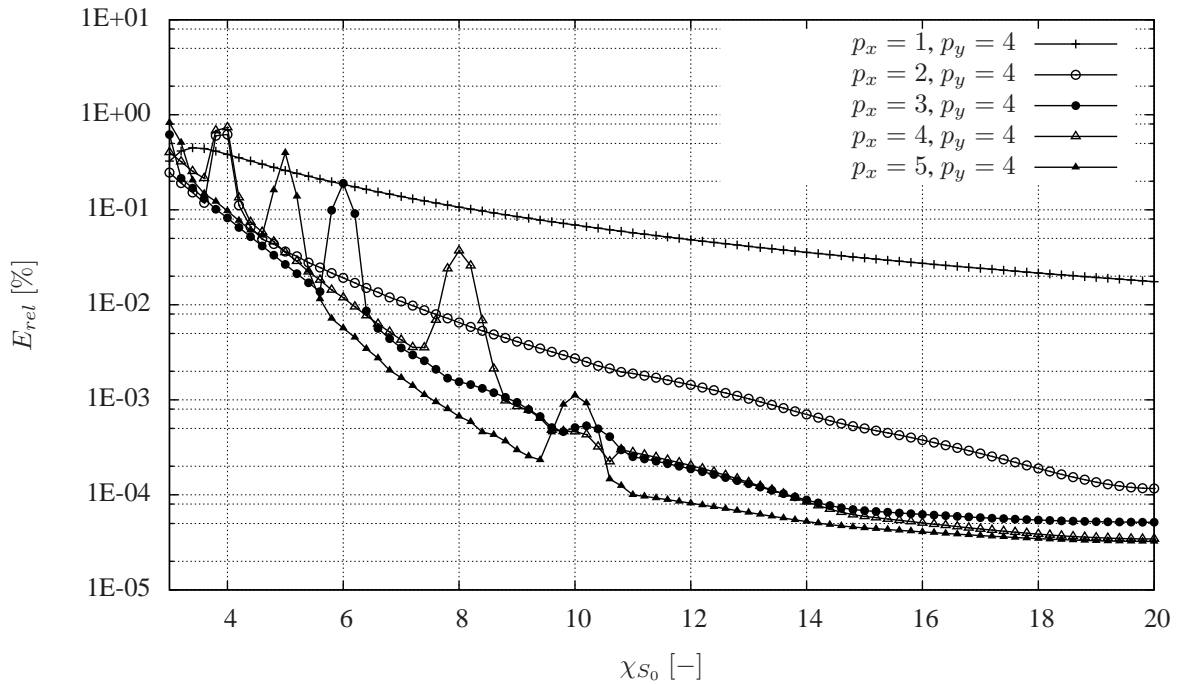


Figure 9: Results of the convergence study for the fundamental symmetric Lamb wave mode are depicted. The model has been discretized using  $p$ -version finite elements. The relative error in group velocity is given over the number of modes per symmetric wavelength ( $\lambda_{S_0}$ ).

Even if the polynomial degree is increased to  $p = 8$  the non-physical oscillations are not notably reduced. The results of the convergence analysis for  $p = 6, 7, 8$  are illustrated in Fig. 10. Different ideas need to be developed therefore in order to avoid these disturbances.

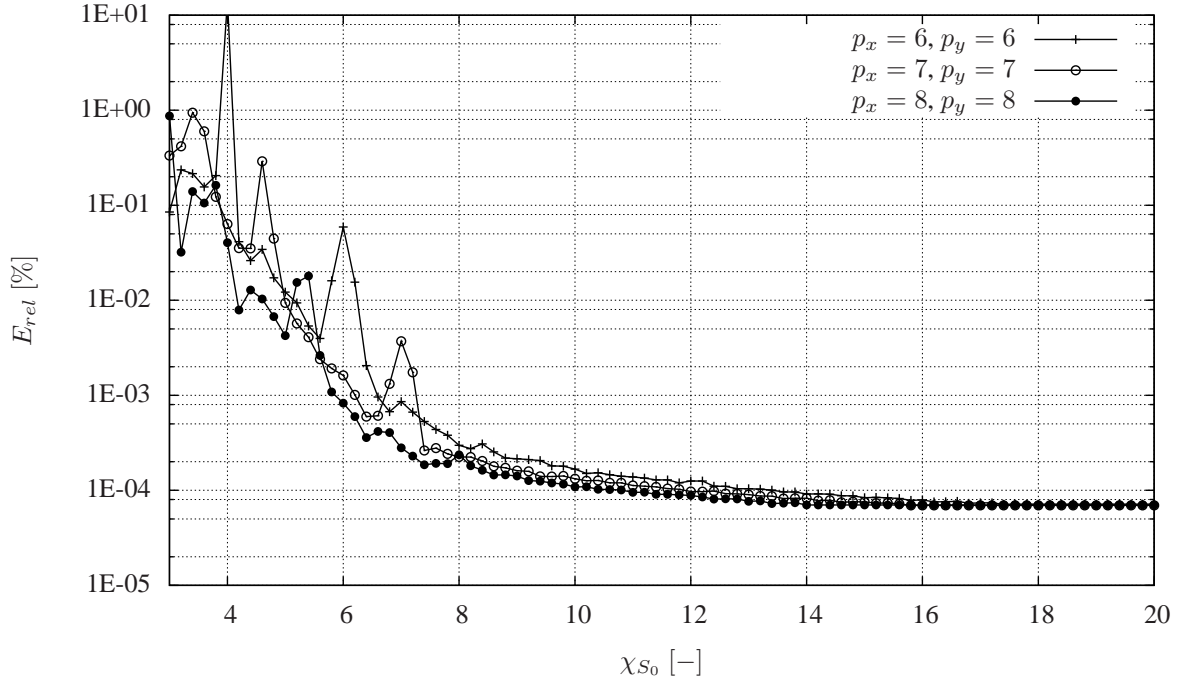


Figure 10: Results of the convergence study for the fundamental symmetric Lamb wave mode are depicted. The model has been discretized using spectral element method. The relative error in group velocity is given over the number of nodes per symmetric wavelength ( $\chi_{S_0}$ ). An isotropic Ansatz space with higher polynomial degrees is testes.

Fig. 11 illustrates the displacement history recorded at point A ( $u_{x,A}$ ). The results are based on computations employing the spectral element method using the polynomial degree template  $p_x = 3, p_y = 4$  and the different values of the number of nodes/modes per wavelength  $\chi_{S_0} = 5, 6$  and  $7$ . Considering Figs. 8 and 9 the displacement signal at  $\chi_{S_0} = 6$  is expected to be significantly distorted. Studying the second diagram of Fig. 11 ( $\chi_{S_0} = 6$ ) we observe stationary oscillations over time. That is to say that point A experiences a standing wave similar to that familiar from a modal analysis. As the group velocity of the fundamental symmetric Lamb wave mode is known a priori, we can conclude that after  $t = 7 \cdot 10^{-5}$  s no oscillations ought to occur at point A. This behavior can accordingly be described as non-physical.

We would like to mention, however, that even simulations using a coarser grid  $\chi_{S_0} = 5$  result in accurate displacement histories. To sum up, if the discretization is refined or coarsened, accurate signals are computed. In principle, therefore, the shape functions are able to resolve the wave form correctly for all three meshes. Moreover, Fig. 11 suggests that the group velocity is not affected by the observed phenomenon. That is to say, signal processing methods, such as the continuous wavelet transform, do not see this effect. From a modelling point of view, however, it is interesting to investigate the source of these oscillations and to devise a remedy. In this way, the analyst can be sure that the results obtained are accurate and there are no numerical artefacts to pollute the simulation results.

In order to identify the source of the described phenomenon, it is helpful to consider the mode shape of the remaining vibrations. Fig. 12 depicts a contour plot of the displacement field for  $\chi_{S_0} = 6$ . In view of the mode shape of the oscillations, the analyst might be reminded of the well-known hourglass phenomenon. This effect is usually seen in low order  $h$ -type finite elements. In this case, efforts are made to avoid shear-locking by integrating special terms of the stiffness matrix deliberately using too few quadrature points. This procedure is called under-integration and is itself another source of errors resulting in zero-energy modes or hourglass modes (Zienkiewicz and Taylor, 2000a). In other words, no energy is needed to achieve the deformed shape for different displacement configurations. As these oscillations are not suppressed by adding an artificial damping, we can conclude that zero-energy modes do not cause the described effect.

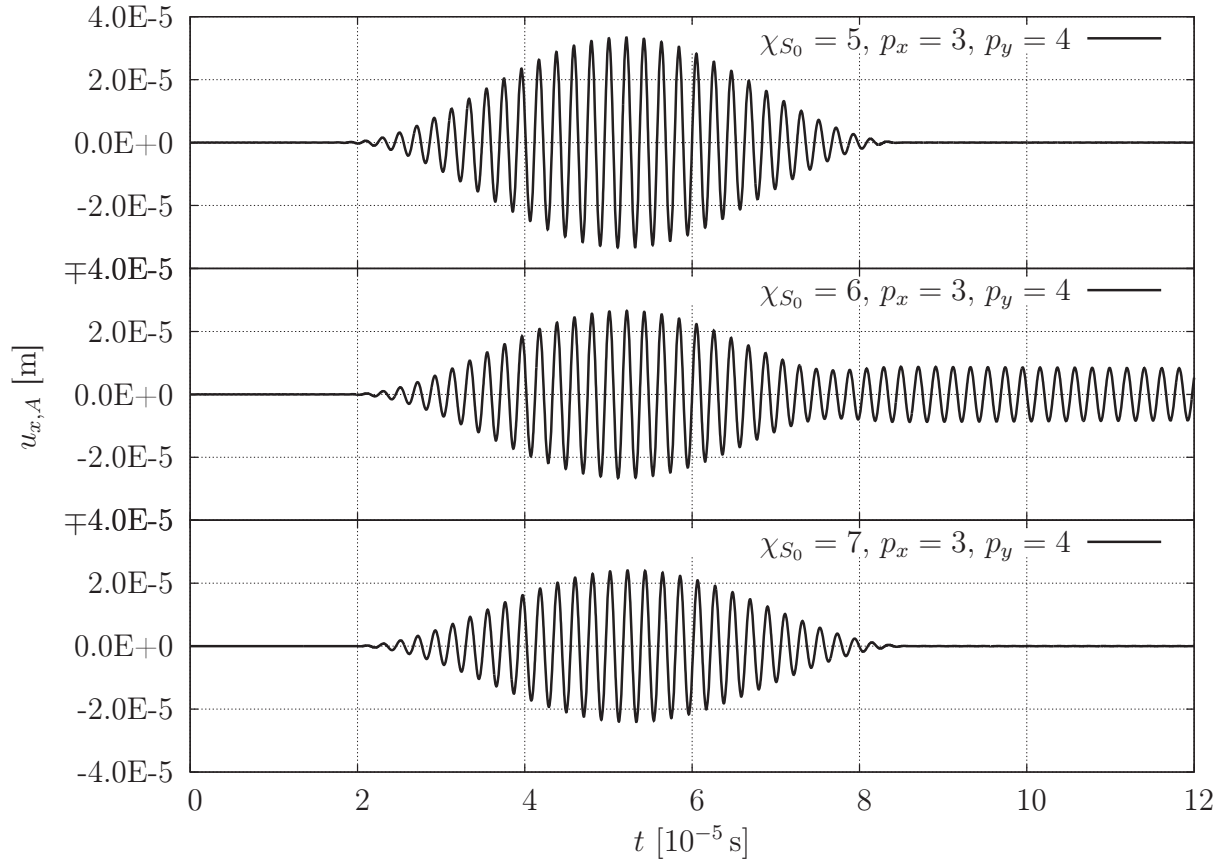


Figure 11: Displacement signal at point A. This depicts the in-plane displacement component  $u_x$ . The results were obtained using the spectral element method with the following polynomial degree template:  $p_x = 3$  and  $p_y = 4$ . Please note, however, if the amount of nodes per symmetric wavelength is chosen to be twice the polynomial degree in propagation direction,  $\chi_{S_0} = 6$ , the solution is evidently corrupted.

After ruling out hourglass modes as a possible source of these errors, a second obvious idea is that the eigen-dynamics of the numerical model might cause such vibrations. In order to prove this assumption, we conduct several modal analyses in the following sub-sections.

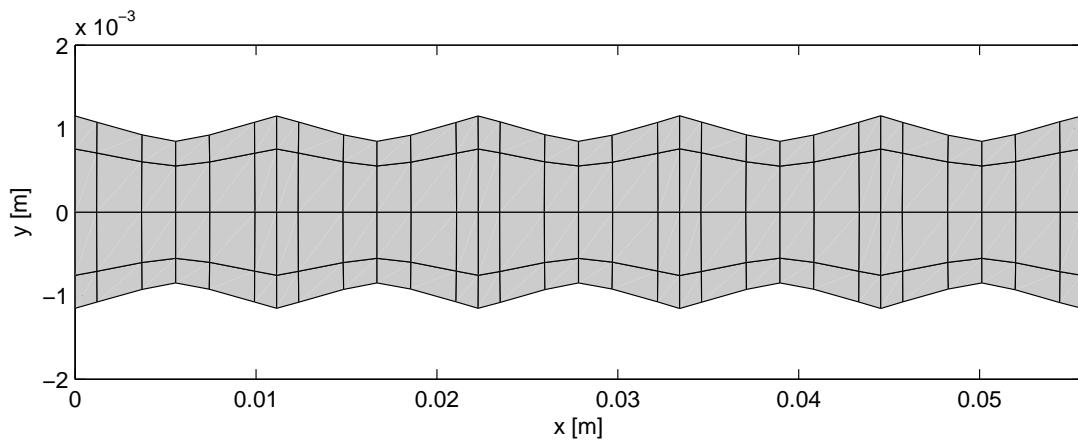


Figure 12: Snapshot of the spurious oscillation components remaining in the plate after the primary wave has already passed. The simulation was conducted using the SEM with  $p_x = 3$ ,  $p_y = 4$  and  $\chi_{S_0} = 6$ . Contour plot corresponding to the graph in the middle row of Fig. 11.

## 5 Modal Analysis of Single Elements and Sub-Models

As a next step in the investigation of this effect, we conduct a modal analysis of a single finite element. It seems likely that elemental eigenfrequencies are excited. Owing to the fact that no physical damping is introduced and that the chosen time integration scheme does not add any numerical damping, the observed vibrations do not vanish. Taking the connection between adjacent finite elements into account, we apply symmetry boundary conditions to its left-hand and right-hand side boundaries. All subsequent considerations are therefore based on the numerical model depicted in Fig. 13. It consists of one element with a variable element width  $b_e$ . The natural frequencies are calculated to solve the well-known linear eigenvalue problem

$$(\mathbf{K} - \omega^2 \mathbf{M}) \hat{\mathbf{v}} = \mathbf{0} \quad (21)$$

with  $\hat{\mathbf{v}}$  describing the mode shape.

**Modal analysis of a single finite element** The results presented in this section are obtained with the aid of the spectral element method. We wish to mention, however, that the same conclusions can be drawn in cases where the  $p$ -version of the finite element method is used.

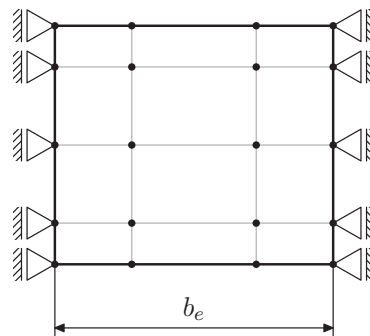


Figure 13: Model for the modal analysis is a single finite element with symmetric boundary conditions.

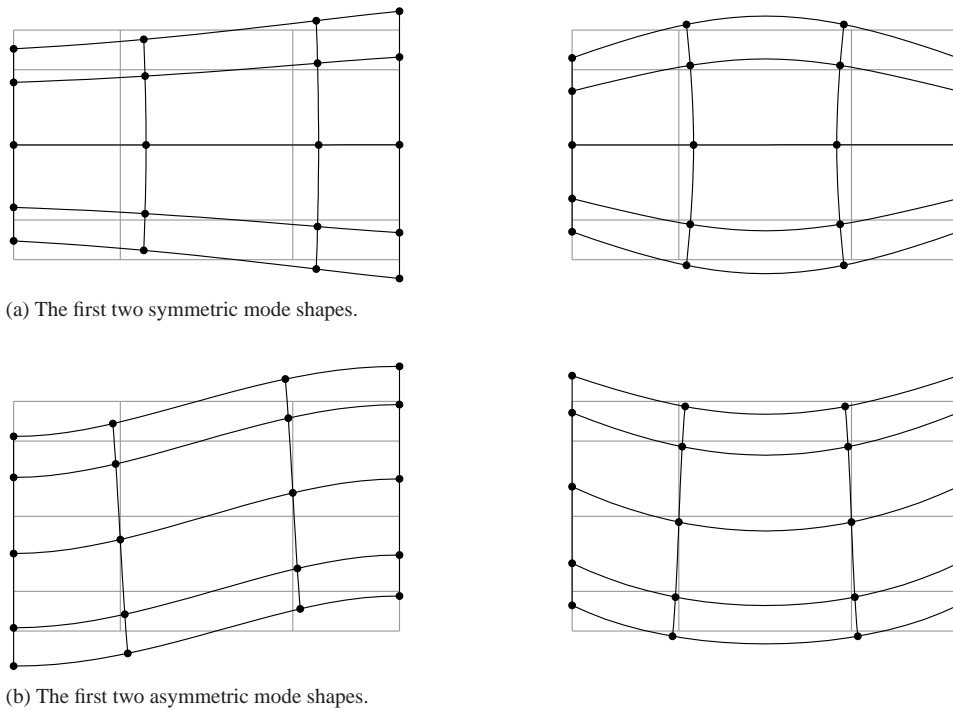


Figure 14: The first two symmetric and asymmetric mode shapes belonging to non-zero eigenvalues of one spectral element with symmetry boundary conditions, cf. Fig. 13. The polynomial degrees are chosen as:  $p_x = 3$ ,  $p_y = 4$ . The element size is  $b_e = 5.568 \cdot 10^{-3}$  m.

Fig. 14a depicts the first two symmetric mode shapes of one individual spectral element using the polynomial degrees  $p_x = 3$ ,  $p_y = 4$  and having an element size of  $b_e = 5.568 \cdot 10^{-3}$  m corresponding to  $\chi_{S_0} = 6$ . A visual inspection of the results, in which the mode shapes are compared with the displacement field in Fig. 12, reveals a qualitative agreement between the first eigenvector and the vibrations. This can be taken as an initial clue to verify the stated assumption. Fig. 14b displays the first two asymmetric mode shapes. As they do not coincide with the oscillations, we just disregard them in the following investigations.

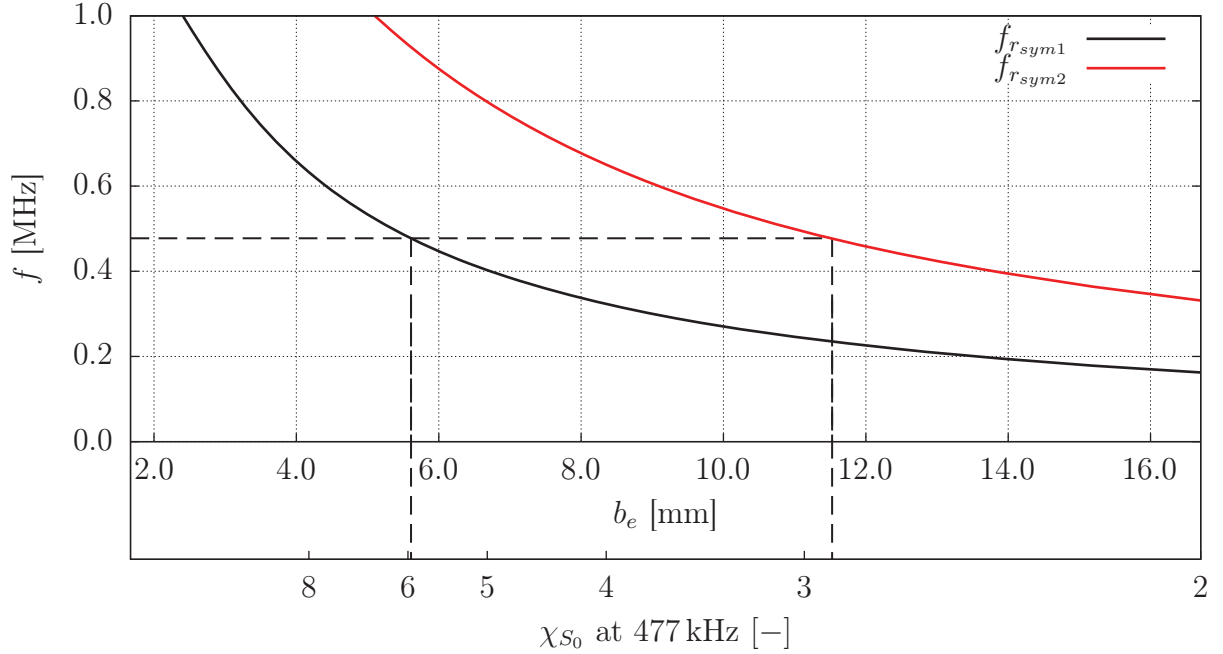


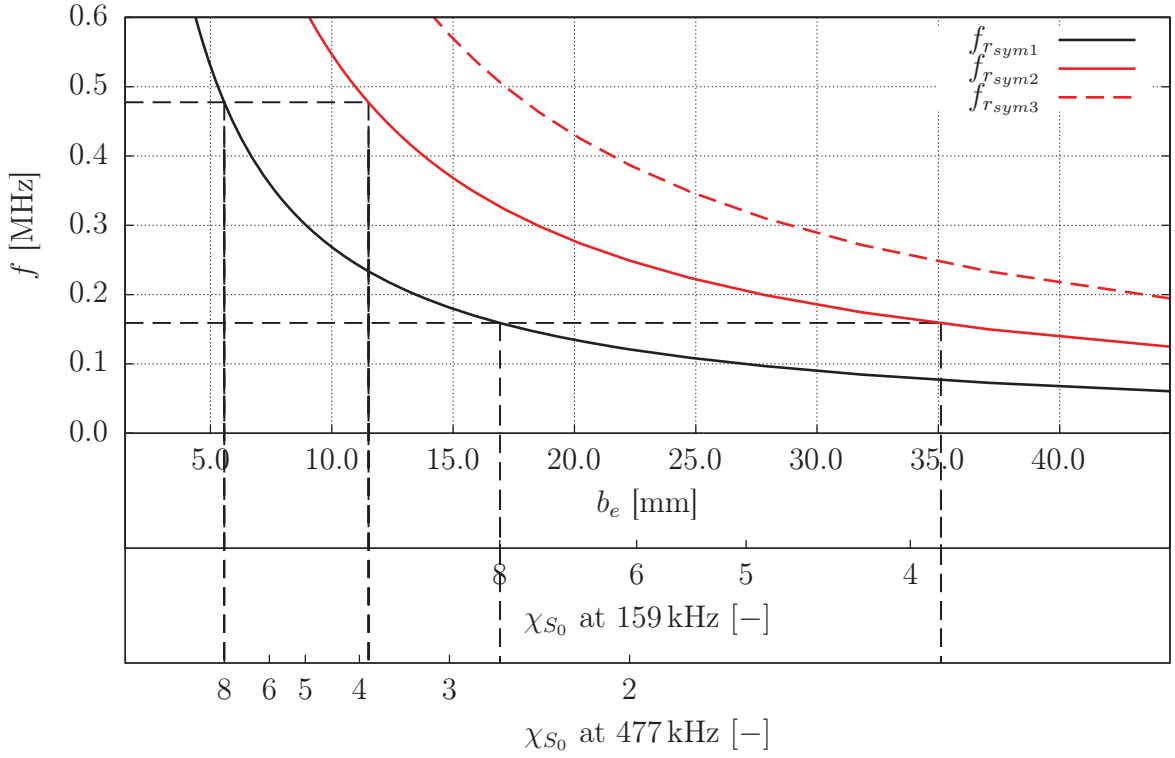
Figure 15: The relation between the first two symmetric element eigenfrequencies of a single spectral element and the element size is illustrated. The polynomial degree template is:  $p_x = 3$  and  $p_y = 4$ .

Fig. 15 plots the symmetric element eigenfrequencies  $f_{r_{symi}}$  as a function of the element width  $b_e$  and the number of nodes per wavelength, respectively. For the sake of clarity, we give both abscissas although they can be easily converted, cf. Eq. (20). At the chosen excitation frequency of  $f_D = 477$  kHz a horizontal line is plotted in the diagram. The intersection of this line with the graphs of the symmetric element eigenfrequencies  $f_{r_{symi}}(b_e)$  gives the critical element sizes at which non-physical vibrations are to be expected. The first critical element width is  $b_e = 5.61$  mm ( $\chi_{S_0} = 2.899$ ) and the second is  $b_e = 11.53$  mm ( $\chi_{S_0} = 5.956$ ). These points coincide with the locations of the peaks seen in Figs. 9 and 8. Consequently, the discovered phenomenon is referred to as *the internal element eigenfrequency effect*.

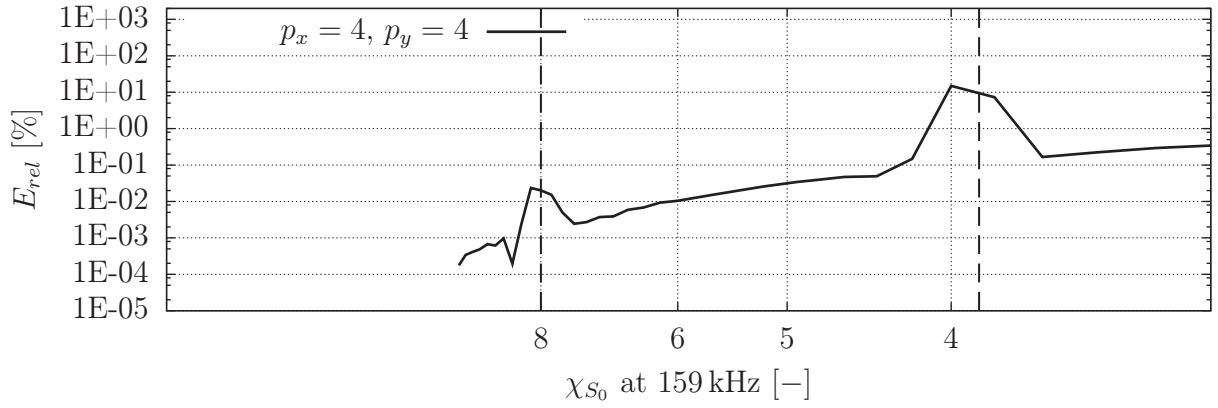
**Frequency dependency of the internal element eigenfrequency effect** The following paragraphs investigate two different excitation frequencies. The wave is excited at  $f_D = 4.77 \cdot 10^5$  Hz and  $f_D = 1.59 \cdot 10^5$  Hz, respectively. The polynomial degrees are chosen as  $p_x = 4$  and  $p_y = 4$ .

Figs. 16b and 16c depict the relative error in group speed for the chosen excitation frequencies and polynomial degree template. We conclude that  $\chi_{S_0} = 3.9$  and  $\chi_{S_0} = 8$  are critical discretization settings. However, it is surprising that the excitation frequency does not seem to have any influence on the critical number of nodes per wavelength. Since the  $x$ -direction is discretized with a shape function of polynomial order  $p_x = 4$  the connection between the polynomial degree in wave propagation direction and the critical  $\chi_{S_0}$ -value is again evident.

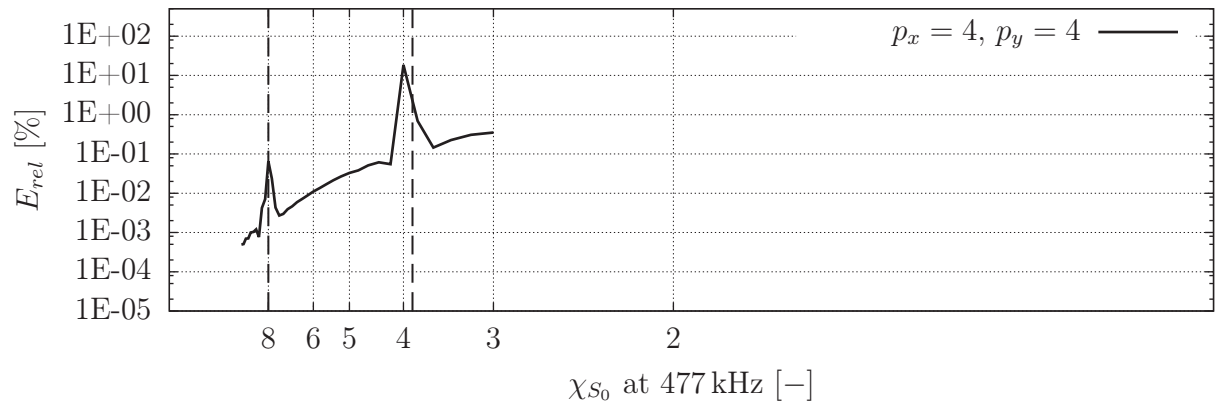
For this reason, we introduce three abscissas that correspond to the element size  $b_e$  and  $\chi_{S_0}$  for the two excitation frequencies (cf. Eq. (20)). Despite the change in the excitation frequency, the locations of the peaks are hardly influenced. Again, the locations of the peaks in the convergence plots for the group velocity are in excellent agreement with the predicted element size due to the elemental eigenfrequency effect.



(a) The relation between the first three symmetric element eigenfrequencies of a single spectral element and the element size is illustrated. The polynomial degree template is:  $p_x = 3$  and  $p_y = 4$ . Where the eigenfrequencies correspond to the excitation frequency, distinct peaks in the convergence curves are observed, cf. Figs. 16a and Fig. 16b.



(b) Convergence curve of the relative error in group velocity for the fundamental symmetric Lamb wave mode. The polynomial degree template is:  $p_x = 4, p_y = 4$ . The excitation frequency is  $f_D = 1.59 \cdot 10^5$  Hz.



(c) Convergence curve of the relative error in group velocity for the fundamental symmetric Lamb wave mode. The polynomial degree template is:  $p_x = 4, p_y = 4$ . The excitation frequency is  $f_D = 4.77 \cdot 10^5$  Hz.

Figure 16: Relation between elemental eigenfrequencies and peaks in the convergence curves.

**Modal analysis of a group of finite elements** So far, it has been implicitly assumed that the structure under investigation is discretized using a regular Cartesian mesh. This can often be the case where thin-walled plate-like structures are concerned. To be applicable for a wider range of problem classes, however, it is necessary to add one last step to the current studies and to look at periodic meshes. This means that adjacent finite elements do not necessarily have to have the same element sizes. Nonetheless, it is possible to extract representative sub-structures from the model. To this end, we proceed to analyze the sub-model depicted in Fig. 17. This sub-structure consists of three spectral elements with varying dimensions  $[1.0 \cdot b_e, 0.7 \cdot b_e, 1.3 \cdot b_e]$ .

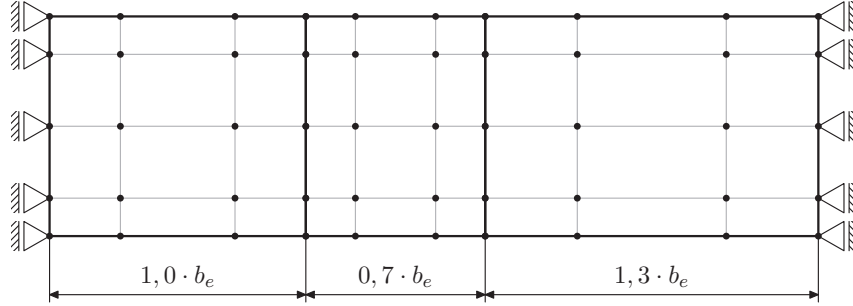


Figure 17: Numerical model for the modal analysis of a periodic sub-structure.

To facilitate the comparison between the results, we use the same mean number of nodes/modes per wavelength as with the simulations discussed in the previous sections. The polynomial degrees are  $p_x = 3$  and  $p_y = 4$ , cf. Fig. 17. As explained before, we begin by computing the symmetric eigenfrequencies of the sub-model as a function of the element width  $b_e$ . The results are illustrated in Fig. 18a. The critical values of  $\chi_{S_0}$  are determined to be 5.92, 8.98 and 18.00. We then proceed to extend the sub-model periodically and study its convergence behavior. As predicted in the modal analysis, irregularities arise at  $\chi_{S_0} = 5.92, 8.98$  and 18.00, cf. Fig. 18b. We can therefore conclude that, even in cases where adjacent elements do not share the same dimensions, the wave propagation analysis can be corrupted. Consequently, the analyst also has to be aware of the eigenfrequency effect described above when employing a periodic mesh. This phenomenon is more pronounced if a coarse discretization is chosen in conjunction with a mono-frequent excitation. Looking at Fig. 18b, we notice that the effect of the disturbed convergence behavior is minimized for a fine spatial discretization. However, this is only the case in a nodes/modes per wavelength range that is of no interest to the practical engineer. The required discretization is too fine so the computational costs are too high. An accuracy of approximately 1% is normally sufficient from an engineering point of view. It is accordingly very important to ensure that the external excitation frequency does not coincide with any internal eigenfrequency.

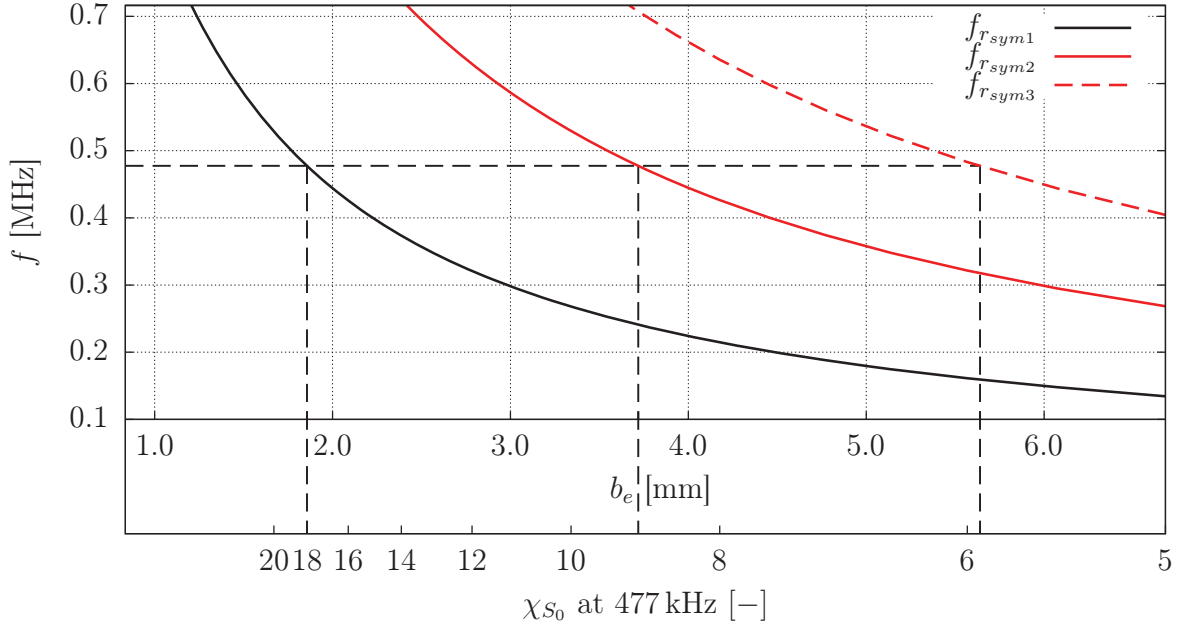
**Guideline to avoid the internal element eigenfrequency effect** The steps given below are designed to help analysts to avoid non-physical oscillations in wave propagation analyses:

1. Determine the size of a single finite element (Cartesian grid) or the size of the smallest representative sub-structure.
2. Apply symmetry boundary conditions to the left-hand and right-hand boundaries.
3. Conduct a modal analysis of the representative sub-structure where the element size is an independent parameter.
4. Extract the symmetric eigenfrequencies.
5. Find the intersection of the excitation frequency with the first symmetric eigenfrequencies. This step determines the critical element sizes  $b_{e,crit}$ .
6. Ensure that the element dimensions  $b_e$  are not coincidental with the critical one.

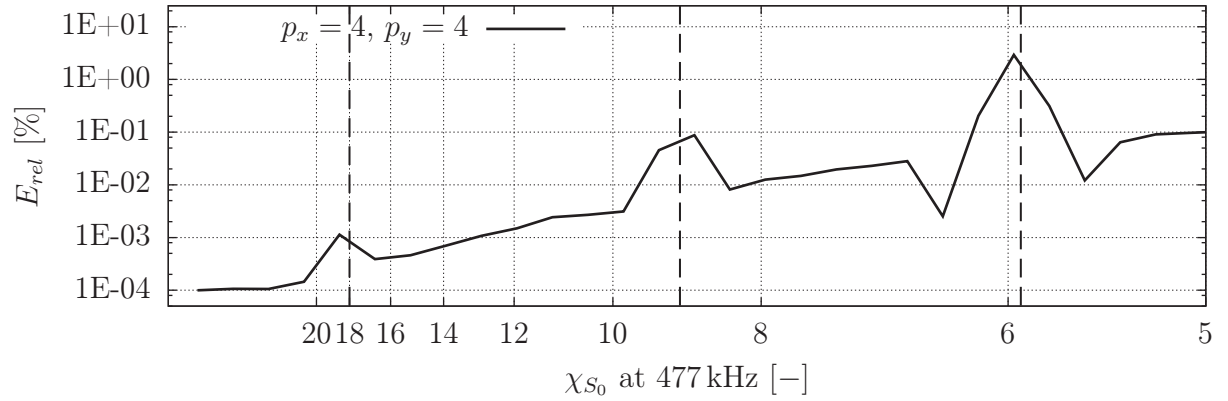
The analyst can easily avoid the internal element eigenfrequency effect and achieve accurate simulations if he adheres to the proposed guideline. If commercial mesh generators and unstructured discretizations are used it is improbable that the observed effect will play a significant role. From the authors' point of view at least, it is

nonetheless essential to be aware of all the pitfalls that may be encountered when dealing with the analysis of guided ultrasonic waves.

It should be mentioned however, that the described phenomenon can also be prevented if unstructured meshes are deployed. Concerning the quality of the simulations it is nonetheless recommended to use finite elements with low aspect ratios. Cartesian grids are accordingly preferred. The analyst consequently tries to partition the model under investigation in order to create regions where a structured, mapped mesh can be applied. It is therefore advised to adhere to the proposed guideline.



(a) The relation between the first three symmetric element eigenfrequencies of a periodic SEM sub-model and the element size is illustrated. The polynomial degree template is:  $p_x = 3$  and  $p_y = 4$ . Where the eigenfrequencies correspond to the excitation frequency, we observe distinct peaks in the convergence curves, cf. Fig. 18b



(b) Convergence curve of the relative error in group velocity for the fundamental symmetric Lamb wave mode. The polynomial degree template is:  $p_x = 4, p_y = 4$ . The excitation frequency is  $f_D = 4.77 \cdot 10^5$  Hz. A periodic sub-model is used.

Figure 18: Relation between elemental eigenfrequencies and peaks in the convergence curves for the sub-model  $[1.0 \cdot b_e, 0.7 \cdot b_e, 1.3 \cdot b_e]$ .

It could be argued, however, that the peaks seen in the convergence curves are merely the results of an offset of the time signal envelope's centroid that was computed using the Hilbert-transform. The phenomenon under investigation has no effect on either the group and phase velocity or on the signal amplitudes. This is true and the eigenfrequency effect could indeed be suppressed by introducing different signal processing schemes, such as the CWT. This is not satisfactory from a numerical point of view, however, as the time signal is nevertheless disrupted. We accordingly believe that such effects should be taken into account whenever wave propagation analysis is conducted. Since the remedy for the eigenfrequency effect is fairly simple, it should be the goal of every analyst to avoid such numerical disturbances.

## 6 Conclusions

The current paper investigates the effect of spurious oscillations caused by elemental eigenfrequencies. Using high-order finite element approaches such as the SEM or the hierarchic  $p$ -FEM, we have illustrated that non-physical oscillations can occur under certain conditions. Various modal analyses have shown that these numerical oscillations can be suppressed once the element dimensions fall below a critical maximum element size, which is smaller than would be inferred from the convergence behavior. To determine these critical mesh sizes, it is necessary to calculate the smallest eigenfrequencies of one element or the smallest periodical sub-model supported by a symmetry boundary conditions. For a proper finite element simulation of the ultrasonic wave propagation in thin-walled structures, it is therefore important to avoid the effects described above, as they may seriously disrupt the accuracy of the solution.

**Acknowledgements** The author, S. Duczek, gratefully acknowledges the support given by the German Research Foundation (DFG) under grant (GA 480/13-3).

## References

- Abboud, N. N.; Pinsky, P. M.: Finite element dispersion analysis for the three-dimensional second-order scalar wave equation. *International Journal for Numerical Methods in Engineering*, 35, (1992), 1183–1218.
- Achenbach, J. D.: *Applied Mathematics and Mechanics: Volume 16 Wave Propagation in Elastic Solids*. North-Holland Publishing Company (1987).
- Ainsworth, M.: Discrete dispersion relation for hp-version finite element approximation at high wave number. *SIAM Journal on Numerical Analysis*, 42, (2004), 553–575.
- Ainsworth, M.; Wajid, H. A.: Dispersive and dissipative behavior of the spectral element method. *SIAM Journal on Numerical Analysis*, 47, (2010a), 3910–3937.
- Ainsworth, M.; Wajid, H. A.: Optimally blended spectral-finite element scheme for wave propagation and non-standard reduced integration. *SIAM Journal on Numerical Analysis*, 48, (2010b), 346–371.
- Babuška, I.; Szabó, B. A.; Katz, I. N.: The p-version of the finite element method. *Journal of Numerical Analysis*, 18, (1981), 515–545.
- Baek, E.; Yim, H.: Numerical modeling and simulation for ultrasonic inspection of anisotropic austenitic welds using the mass-spring lattice model. *NDT & E International*, 44, (2011), 571–582.
- Bathe, K. J.: *Finite-Elemente-Methoden*. Springer Verlag (2002).
- Christon, M. A.: The influence of the mass matrix on the dispersive nature of the semi-discrete, second-order wave equation. *Computer Methods in Applied Mechanics and Engineering*, 173, (1999), 147–166.
- Dauksher, W.; Emery, A. F.: Accuracy in modeling the acoustic wave equation with Chebyshev spectral finite elements. *Finite Elements in Analysis and Design*, 26, (1997), 115–128.
- Dauksher, W.; Emery, A. F.: An evaluation of the cost effectiveness of Chebyshev spectral and p-finite element solutions to the scalar wave equation. *International Journal for Numerical Methods in Engineering*, 45, (1999), 1099–1113.
- De Basabe, J. D.; Sen, M. K.: Grid dispersion and stability criteria of some common finite-element methods for acoustic and elastic wave equations. *Geophysics*, 72, (2007), T81–T95.
- Demkowicz, L.: *Computing with hp-Adaptive Finite Elements: Volume 1: One and Two Dimensional Elliptic and Maxwell Problems*. Chapman and Hall (2006).
- Demkowicz, L.; Kurtz, J.; Pardo, D.; Paszynski, M.; Rachowicz, W.; Zdunek, A.: *Computing with hp-Adaptive Finite Elements: Volume 2 Frontiers: Three Dimensional Elliptic and Maxwell Problems with Applications*. Chapman and Hall (2008).
- Duczek, S.; Gabbert, U.: Anisotropic hierarchic finite elements for the simulation of piezoelectric smart structures. *Engineering Computations*, 30, (2013), 21pp.

- Düster, A.: *High Order Finite Elements for Three-Dimensional, Thin-Walled Nonlinear Continua*. Ph.D. thesis, Technical University of Munich (2002).
- Eds.: Boller, C.; Chang, F.-K.; Fujino, Y.: *Encyclopedia of Structural Health Monitoring*. John Wiley & Sons (2009).
- Fichtner, A.: *Full Seismic Waveform Modelling and Inversion*. Springer Verlag (2011).
- Fish, J.; Belytschko, T.: *A First Course in Finite Elements*. John Wiley and Sons (2007).
- Giurgiutiu, V.: *Structural Health Monitoring with Piezoelectric Active Wafer Sensors: Fundamentals and Applications*. Elsevier (2008).
- Graff, K. F.: *Wave Motion in Elastic Solids*. Oxford University Press (1975).
- Ha, S.; Chang, F.-K.: Optimizing a spectral element for modeling PZT-induced Lamb wave propagation in thin plates. *Smart Materials and Structures*, 19, (2010), 1–11.
- Hamel, G.: *Theoretische Mechanik*. Springer (1967).
- Hughes, T. J. R.: *The Finite Element Method: Linear Static and Dynamic Finite Element Analysis*. Prentice-Hall (1987).
- Ihlenburg, F.; Babuška, I.: Dispersion analysis and error estimation of Galerkin finite element methods for the numerical computation of waves. *International Journal for Numerical Methods in Engineering*, 38, (1995a), 3745–3774.
- Ihlenburg, F.; Babuška, I.: Finite element solution of the Helmholtz equation with high wave number part I: The h-version of FEM. *Computer and Mathematics with Applications*, 30, (1995b), 9–37.
- Ihlenburg, F.; Babuška, I.: Finite element solution of the Helmholtz equation with high wave number part II: The hp-version of FEM. *SIAM Journal on Numerical Analysis*, 34, (1997a), 315–358.
- Ihlenburg, F.; Babuška, I.: Reliability of finite element methods for the numerical computation of waves. *Advances in Engineering Software*, 28, (1997b), 417–424.
- Jensen, M. S.: High convergence order finite elements with lumped mass matrix. *International Journal for Numerical Methods in Engineering*, 39, (1996), 1879–1888.
- Komatitsch, D.; Tromp, J.: Spectral-element simulations of global seismic wave propagation - I. Validation. *International Journal of Geophysics*, 149, (2002), 390–412.
- Kudela, P.; Krawczuk, M.; Ostachowicz, W.: Wave propagation modelling in 1d structures using spectral elements. *Journal of Sound and Vibration*, 300, (2006), 88–100.
- Lamb, H.: On waves in an elastic plate. *Proceedings of the Royal Society of London. Series A*, 93, 648, (1917), 114–128.
- Lee, B. C.; Staszewski, W. J.: Lamb wave propagation modelling for damage detection: I. Two-dimensional analysis. *Smart Materials and Structures*, 16, (2007a), 249–259.
- Lee, B. C.; Staszewski, W. J.: Lamb wave propagation modelling for damage detection: II. Damage monitoring strategy. *Smart Materials and Structures*, 16, (2007b), 260–274.
- Leung, A. Y. T.; Chan, J. K. W.: Fourier p-element for the analysis of beams and plates. *Journal of Sound and Vibration*, 212, (1997), 179–185.
- Leung, A. Y. T.; Zhu, B.: Hexahedral Fourier p-elements for vibration of prismatic solids. *International Journal of Structural Stability and Dynamics*, 4, (2003), 125–138.
- Mulder, W. A.: Spurious modes in finite-element discretizations of the wave equation may not be all that bad. *Applied Numerical Mathematics*, 30, (1999), 425–445.
- Mullen, R.; Belytschko, T.: Dispersion analysis of finite element semidiscretizations of the two-dimensional wave equation. *International Journal for Numerical Methods in Engineering*, 18, (1982), 11–29.
- Ostachowicz, W.; Kudela, P.; Krawczuk, M.; Zak, A.: *Guided Waves in Structures for SHM: The Time-Domain Spectral Element Method*. John Wiley & Sons (2011).

- Park, K. C.; Flaggs, D. L.: A Fourier analysis of spurious mechanisms and locking in the finite element method. *Computer Methods in Applied Mechanics and Engineering*, 46, (1984), 65–81.
- Patera, A. T.: A spectral element method for fluid dynamics: Laminar flow in a channel expansion. *Journal of Computational Physics*, 54, (1984), 468–488.
- Peng, H.; Meng, G.; Li, F.: Modeling of wave propagation in plate structures using three-dimensional spectral element method for damage detection. *Journal of Sound and Vibration*, 320, (2009), 942–954.
- Pozrikidis, C.: *Introduction to Finite and Spectral Element Methods Using MATLAB*. Chapman & Hall/CRC (2005).
- Raghavan, A.; Cesnik, C. E. S.: *Damage Prognosis: For Aerospace, Civil and Mechanical Systems*, chap. 11, pages 235–258. John Wiley and Sons (2005).
- Rose, J. L.: *Ultrasonic Waves in Solid Media*. Cambridge University Press (1999).
- Seriani, G.: 3-d large-scale wave propagation modeling by spectral element method on cray t3e multiprocessor. *Computer Methods in Applied Mechanics and Engineering*, 164, (1998), 235–247.
- Seriani, G.; Oliveira, S. P.: DFT modal analysis of spectral element methods for acoustic wave propagation. *Journal of Computational Acoustics*, 16, (2008a), 531–561.
- Seriani, G.; Oliveira, S. P.: Dispersion analysis of spectral element methods for elastic wave propagation. *Wave Motion*, 45, (2008b), 729–744.
- Seriani, G.; Priolo, E.: Spectral element method for acoustic wave simulation in heterogeneous media. *Finite Elements in Analysis and Design*, 16, (1994), 337–348.
- Solin, P.; Segeth, K.; Dolezel, I.: *Higher-Order Finite Element Methods*. Chapman and Hall (2004).
- Su, Z.; Ye, L.: *Lecture Notes in Applied and Computational Mechanics: Volume 48 Identification of Damage Using Lamb Waves*. Springer Verlag (2009).
- Szabó, B.; Babuška, I.: *Finite Element Analysis*. John Wiley and Sons (1991).
- Szabó, B.; Babuška, I.: *Introduction to Finite Element Analysis: Formulation, Verification and Validation*. John Wiley and Sons (2011).
- Thompson, L. L.; Pinsky, P. M.: Complex wavenumber Fourier analysis of the p-version finite element method. *Computational Mechanics*, 13, (1994), 255–275.
- Viktorov, I. A.: *Rayleigh and Lamb Waves*. Plenum Press. (1967).
- Weinberg, K.: *Ein Finite-Elemente-Konzept zur lokalen Netzverdichtung und seine Anwendung auf Koppel- und Kontaktprobleme*. Ph.D. thesis, Otto-von-Guericke-University of Magdeburg (1996).
- Willberg, C.: *Development of a New Isogeometric Finite Element and its Application for Lamb Wave Based Structural Health Monitoring*. VDI Fortschritt-Berichte Reihe 20 Nr. 446 (2013).
- Willberg, C.; Duczek, S.; Vivar-Perez, J. M.; Schmicker, D.; Gabbert, U.: Comparison of different higher order finite element schemes for the simulation of Lamb waves. *Computer Methods in Applied Mechanics and Engineering*, 241-244, (2012), 246–261.
- Worlton, D. C.: Ultrasonic flaw detection and means (August 1961).
- Wriggers, P.: *Nonlinear Finite-Element-Methods*. Springer-Verlag (2009).
- Xu, B.; Yu, L.; Giurgiutiu, V.: Advanced methods for time-of-flight estimation with application to Lamb wave structural health monitoring. In: *The 7<sup>th</sup> International Workshop on Structural Health Monitoring 2009* (2009).
- Zak, M.; Krawczuk, M.; W., O.: Propagation of in-plane waves in an isotropic panel with a crack. *Finite Elements in Analysis and Design*, 42, (2006), 929–941.
- Zienkiewicz, O. C.; Taylor, R. L.: *The Finite Element Method: Volume 1 The Basis*. Butterworth Heinemann (2000a).

Zienkiewicz, O. C.; Taylor, R. L.: *The Finite Element Method: Volume 2 Solid Mechanics*. Butterworth Heinemann (2000b).

Zienkiewicz, O. C.; Taylor, R. L.: *The Finite Element Method: Volume 3 Fluid Dynamics*. Butterworth Heinemann (2000c).

---

*Address:* David Schmicker, Sascha Duczek, Steffen Liefold, Ulrich Gabbert  
Otto-von-Guericke-Universität Magdeburg, Institut für Mechanik, D-39106 Magdeburg, Germany  
email: {david.schmicker, sascha.duczek, steffen.liefold, ulrich.gabbert}@ovgu.de